# XMM-Newton CCF Release Note

XMM-CCF-REL-382

## Update of the CORRAREA Empirical EPIC Effective Area Correction

M.J.S. Smith (ESAC), C. Pommranz (IAAT), C. Heinitz (IAAT)
and M. Stuhlinger (ESAC)

July 26, 2021

## 1 CCF Components

| Name of CCF | VALDATE | EVALDATE | Blocks Changed | XSCS Flag |
|---|---|---|---|---|
| XRT1_XAREAEF_0010.CCF | 2000-01-13T00:00:00 | | CORRAREA | No |
| XRT2_XAREAEF_0011.CCF | 2000-01-13T00:00:00 | | CORRAREA | No |
| XRT3_XAREAEF_0013.CCF | 2000-01-13T00:00:00 | | CORRAREA | No |

## 2 Changes

This release contains a recalibration of the empirical MOS-to-pn effective area corrections, originally introduced in September 2014 as the CORRAREA correction [1]. The corrections consist of energy dependent multiplicative functions which modify the standard instrumental effective area curves as produced by the `arfgen` task. The correction is currently not yet applied by default, and the user should invoke it explicitly by running `arfgen` with the parameter `applyxcaladjustment=yes`.

The recalibrated corrections modify the MOS effective areas from 2 keV upwards. Below this energy the MOS effective areas are unchanged. The pn effective area curve is not modified at all.

The correction functions are designed to bring the MOS spectra more in line with the pn by empirically correcting residual calibration issues affecting instrumental throughput, mainly telescope effective areas and detector quantum efficiencies.

The choice to modify the MOS effective areas assuming the pn calibration is essentially arbitrary[1], and thus, although applying the correction will yield a significant improvement in the formal

[1] There are some practical considerations: of the EPIC cameras, the pn has the highest signal-to-noise over much of the band pass and is more readily compared across observatories, and the pn throughput is very stable over time.

consistency between EPIC spectral parameters, it will emphatically not necessarily result in reduced systematic errors. Nevertheless, depending on the science case, applying the CORRAREA correction may allow the user to better exploit the combined EPIC datasets in spectral analysis. Furthermore, the recalibration of the MOS-to-pn corrections is a preparatory step, anticipating a future modification of the pn effective area to a best estimate of the absolute calibration.

The derivation of the correction is described in the following sections. In broad lines, it follows the method presented in [1], which in turn was based on an analysis of the EPIC effective area cross-calibration described in [2], although the analysis presented here contains some important differences in methodology.

### 2.1 Sample selection and data reduction

The calibration is based on a sample of EPIC observations of targets selected from the 3XMM-DR7 catalogue [3], using as main criteria:

- all EPIC exposures are taken in imaging modes;
- the target is identified as a point source;
- the target is located within 2' of the nominal aim-point;
- there is no source confusion;
- mode-dependent count rate limits to ensure the target is sufficiently bright yet not piled-up.

The selected observations were further screened for pile-up, bad columns and other observation specific anomalies. The list of the resulting 120 observations is summarised in Table 1.

Per observation, strictly simultaneous good-time intervals across the EPIC instruments were derived, source and background spectra were extracted (using patterns 0–4 for pn, and 0–12 for MOS - see also Section 4), and spectral products were produced using the standard SAS processing and analysis methods. The source spectra were extracted from circular regions of up to 60" in radius, although where necessary the radius was limited so as not to overlap with chip gaps or lie outside the read-out window. MOS background spectra were selected from a source-free annulus around the source region (minimum inner radius of 90"), or, when this was not feasible, a circular region in an outer area of the central CCD or in a peripheral CCD. The pn background was obtained from a circular region at the same RAWY value as the source and within the central region of the detector (in view of obtaining similar instrumental fluorescent background emission), or, in the case of Small Window mode, from a source free region in the read-out window.

For each observation the best fit model to the pn data was derived - where possible, physically motivated models were used, avoiding as far as feasible the introduction of ad hoc components which may bias spectral comparisons across instruments. Per instrument, all source spectra and model spectra (the latter being the expected counts as per the pn reference model + scaled background counts) were co-added (stacked); the energy ranges contributing to the stacked data were limited

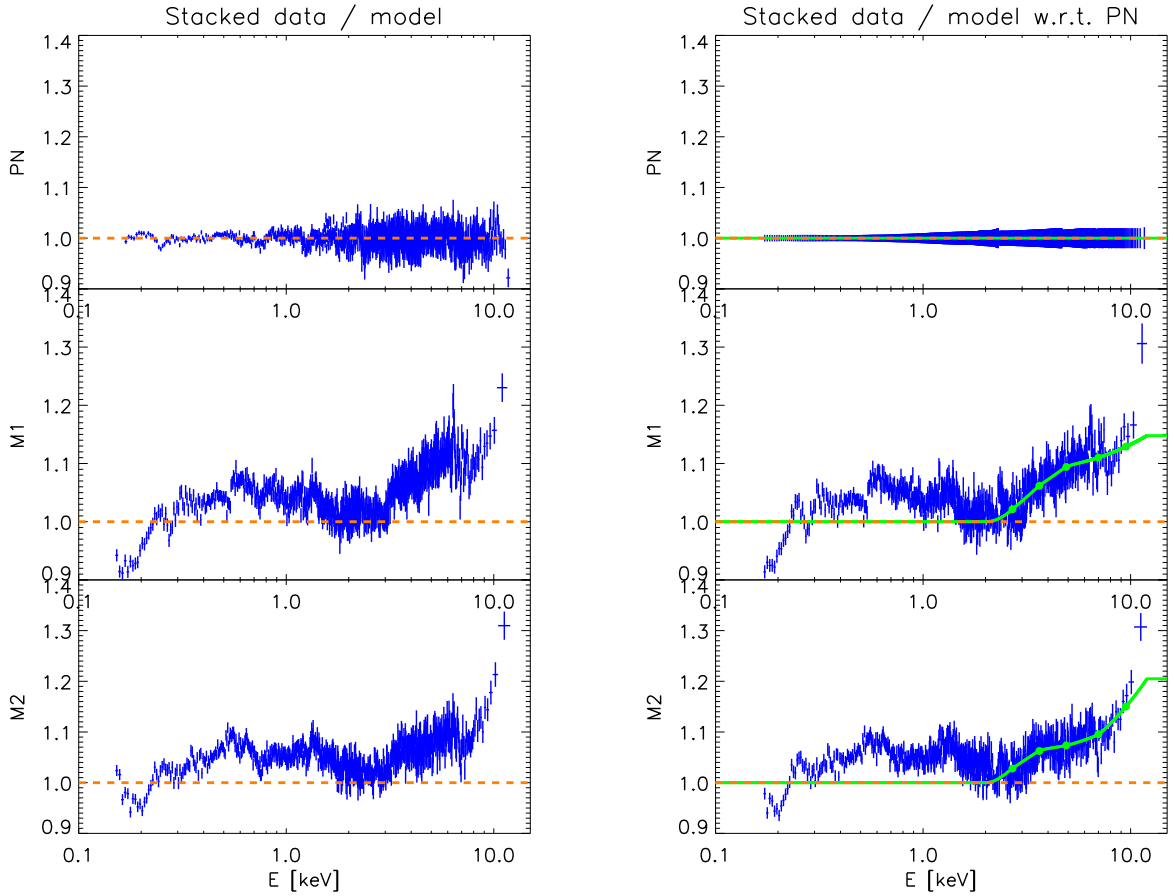


Figure 1: *Left panel:* Instrumental stacked data-to-model ratios (in PI space) with respect to the best fit models to pn data; from top to bottom: pn, MOS1, MOS2. Data are rebinned to a minimum SNR of 50 for the purpose of clarity. *Right panel:* As left panel, but normalised to the stacked data-to-model ratios of the pn. For visual comparison, overlaid in green are the optimised effective area correction curves (in energy space). For pn, a null correction is applied. For the MOS instruments, the respective spline nodes are indicated by the filled circles, which also indicate the statistical 90% confidence intervals.

to those with sufficient signal-to-noise and were determined per observation. The stacking allows to increase overall signal-to-noise, which is especially useful in extending the spectral comparisons towards the higher energy limits of the instrumental band passes. Then the instrumental stacked data-to-model ratios were determined, and normalised to those of the pn (see Fig. 1). These normalised stacked data-to-model ratios provide a useful measure of the cross-calibration, as these values would be unity in the case of a fully consistent MOS versus pn calibration.

## 2.2 Derivation of the CORRAREA correction

The MOS1 and MOS2 effective area corrections are derived independently. Per instrument, the correction is defined by a spline function describing the energy dependent multiplication factors to be applied to the nominal effective area vector. Given the respective MOS spectral products and the pn spectral models, a simultaneous fit was performed across all observations in order to

determine the spline node amplitudes which minimise the normalised stacked data-to-model ratios. The definition of the spline nodes is somewhat arbitrary, their number being a compromise between sufficient resolution and practical computation time, and their locations being adapted to the shape of the required correction.

An important consideration in deriving the correction functions is defining an appropriate energy range over which they should effectively operate. The spectral discrepancies between the EPIC instruments cannot be assumed to be limited to issues with throughput calibration. Other calibration inaccuracies, especially those related to redistribution (and, to a lesser extent, energy scale) will likely contribute significantly and may start to dominate towards lower energies.

A range of correction functions was tested with differing effective energy ranges towards lower energies. These results show that corrections below $\sim$ 2 keV, while improving the average cross-calibration, lead to worsening in a number of individual cases. Investigations show that this is probably due to the low energy calibration issues indeed in part being related to redistribution and thus not possible to be improved through an effective area correction alone. The interdependency of the redistribution and effective area effects at low energies requires more investigation, and hence in this release an effective low-energy bound for the CORRAREA correction is set to 2.0 keV, which is implemented through a smooth transition under condition of continuity to a null correction below that energy.

At energies above $\sim$ 10 keV, a sudden increase in cross-calibration discrepancies is seen for both MOS cameras. Although it cannot a priori be ruled out that this effect is fully related to the overall effective area calibration, there are indications that this issue could be due to software algorithms not properly constraining model extrapolations towards high energies. Indeed, also for pn, despite the stacked data-to-model ratios being close to unity across the whole band, there are significant discrepancies at the very highest energies. This indicates a difficulty in properly modelling the pn spectra at $\sim$ 12 keV. Owing to the possibly different nature of these particular calibration issues, and pending further investigation, it is decided not to take these into account in the current implementation. Thus the CORRAREA correction up to 12 keV is simply an extrapolation of the correction function at 10 keV. From 12 keV upwards the correction is maintained constant.

The correction functions, optimised for the 2.0–10.0 keV band, and as implemented in this release of the CORRAREA correction, are shown overlaid in Fig. 1.

## 3 Scientific Impact of this Update

The normalised stacked data-to-model ratios obtained with and without the CORRAREA correction are compared in Fig. 2. The impact of applying the correction across the sample is further illustrated in Fig. 3 which shows the resulting changes of MOS-to-pn flux ratios with respect to those obtained with the current default effective area files.

The results show a clear improvement in the average MOS-to-pn spectral cross-calibration upwards of 2 keV. With respect to the standard effective area files, applying the correction will result in formally improved simultaneous spectral fits across the EPIC instruments, and more consistent

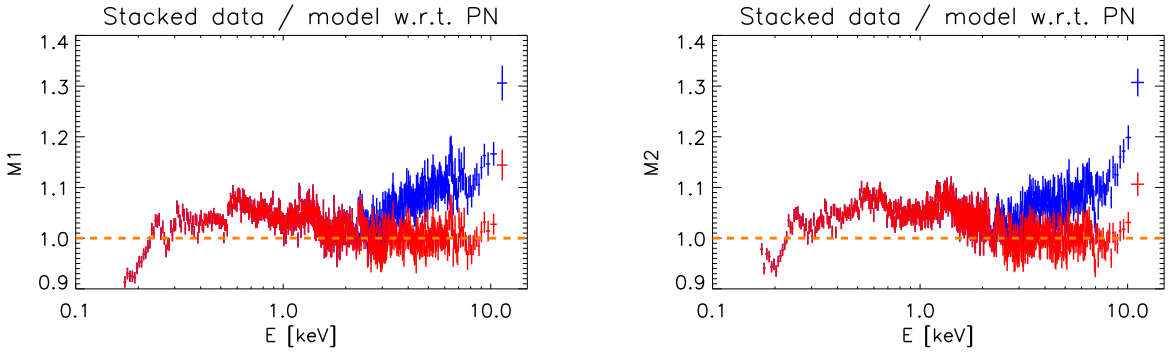


Figure 2: Comparison of the normalised stacked data-to-model ratios obtained with the current default effective area files (shown in blue) and after applying the CORRAREA correction (shown in red). MOS1 and MOS2 are shown in the left and right panels, respectively.

model parameters, especially above 2 keV. However, we emphasize that these improvements do not necessarily imply reduced systematic errors in the MOS data.

Further testing of the CORRAREA correction was performed on several independent data sets. An example is illustrated in Fig. 4, which shows the results obtained from a sample of 42 observations of bright blazars (PKS 2155-304, 3C 273 and H 1426+428). As these sources are generally too bright for EPIC imaging modes, and require pile-up mitigation in spectral analysis, they are less suitable for deriving an effective area correction. Nevertheless, they do serve as useful validations of the calibration. The results are in-line with expectations and confirm the validity of the CORRAREA correction.

The change in MOS fluxes due to the CORRAREA correction is illustrated in Fig. 5. Fluxes below 2 keV are not affected. From 2 keV upwards, MOS on-axis fluxes will gradually decrease by up to $\sim 12\%$ at 10 keV. For relevant power-law components this implies a change of $\sim 0.05$ in terms of index.

Finally, in Fig. 6, we compare MOS-to-pn flux ratios obtained with this CCF release with those obtained with the original CORRAREA correction. For energies above $\sim 2$ keV, the new results yield a similar or much improved consistency between EPIC fluxes. This is partly due to the new extended sample providing more data allowing a modelling of the correction functions beyond the $\sim 7$ keV cut-off used imposed in the original derivation. At energies below $\sim 2$ keV, both corrections show a similar dynamic range in flux discrepancies. With respect to the new results, the original corrections yield MOS-to-pn flux ratios which are offset towards lower values. This is due to the respective levels of the constant correction functions applied in this energy range (with respect to pn, the new correction uses unity, whereas the original corrections are at 4% for MOS1 and 6% for MOS2).

## 4 Estimated Scientific Quality

As mentioned in Section 2.1, the CORRAREA calibration is derived from and optimised for:

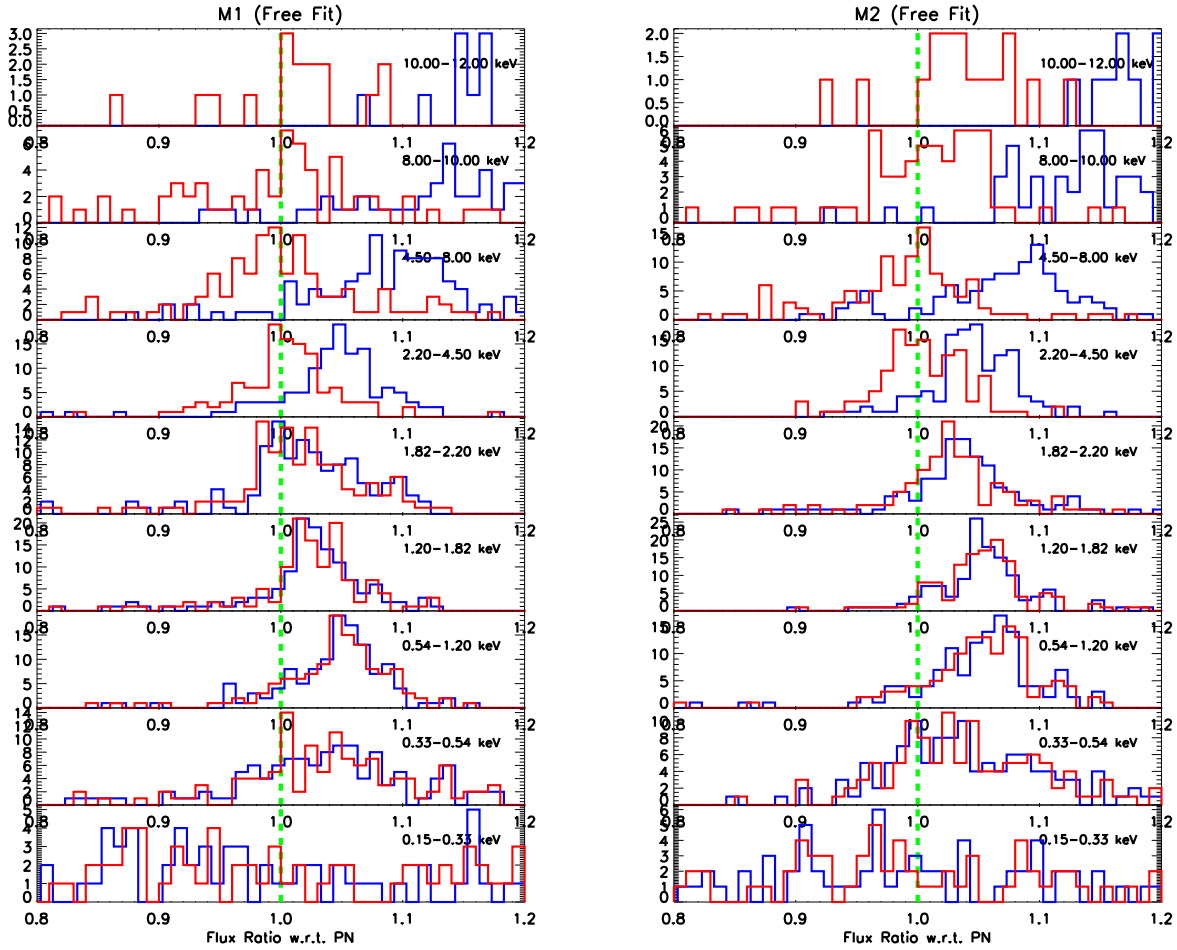


Figure 3: MOS-to-pn flux ratio histograms in several energy bands (top to bottom panels) for the observations in the sample. MOS1 and MOS2 are shown in the left and right panels, respectively. Results obtained with the current default effective area files are shown in blue. Those obtained with the new CORRAREA correction are shown in red. Note that the abscissa range is limited for clarity - there is outlying data, mainly in the very lowest energy band, although with large associated uncertainties in flux ratios.

- on-axis sources (within $\sim 2'$ of the nominal aim-point);
- spectra extracted with patterns 0–4 (singles and doubles) for pn, and 0–12 (singles – quadruples) for MOS.

Recent investigations indicate there are pattern-dependent calibration issues, likely affecting the MOS spectral quality towards higher energies. It is therefore expected that the CORRAREA correction will only yield optimal results for the above mentioned pattern selections.

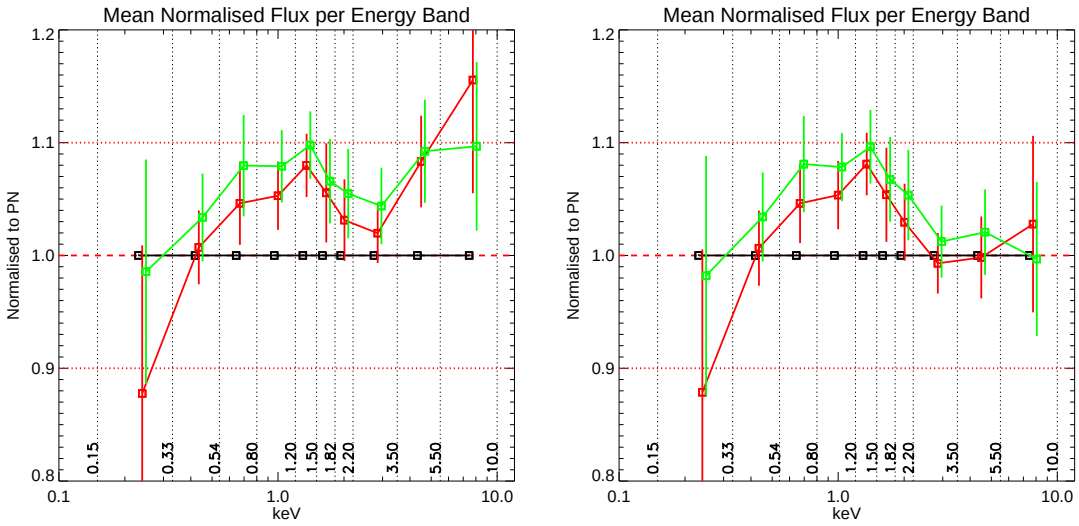


Figure 4: Mean MOS-to-pn flux ratios over a sample of 42 observations of bright blazars. The mean flux ratios are determined in several energy bands. Error bars denote the sample standard deviation. MOS1 and MOS2 results are shown in red and green, respectively. Left panel: results obtained with the current default effective area files. Right panel: results obtained with the new CORRAREA correction.

# 5 Expected Updates

In future versions of the SAS, the CORRAREA correction will likely be applied automatically, without the user needing to explicitly invoke it (i.e. the default setting for `arfgen` will be `applyxcaladjustment=yes`).

There are several issues currently being investigated which may lead to future updates of the CORRAREA correction:

- advances in the EPIC redistribution calibration may inform the effective area calibration below 2 keV;
- a better understanding of the origins of the discrepancies above 10 keV may result in an improved correction;
- investigations into pattern-dependencies may lead to a more general application of the correction.

In addition, future changes to pn or MOS calibration will require a validation and possible recalibration of the CORRAREA correction.

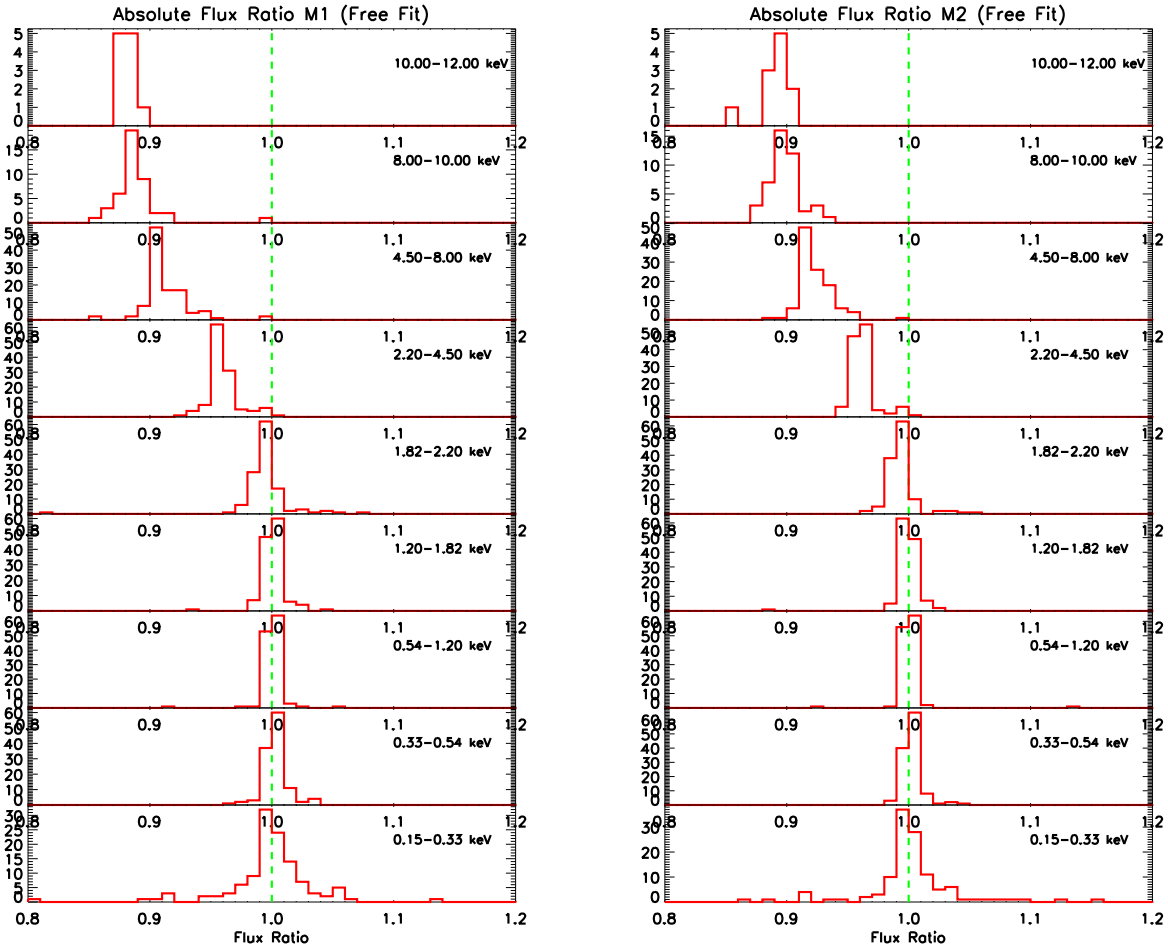


Figure 5: Histograms over the sample of observations of the fractional change in MOS fluxes obtained with the new CORRAREA correction with respect to those obtained with the current default effective area files. MOS1 and MOS2 are shown in the left and right panels, respectively.

# 6 Test Procedures and Summary of Test Results

Functional tests with `cifbuild` and `arfgen` (SAS 19.1) were successful.

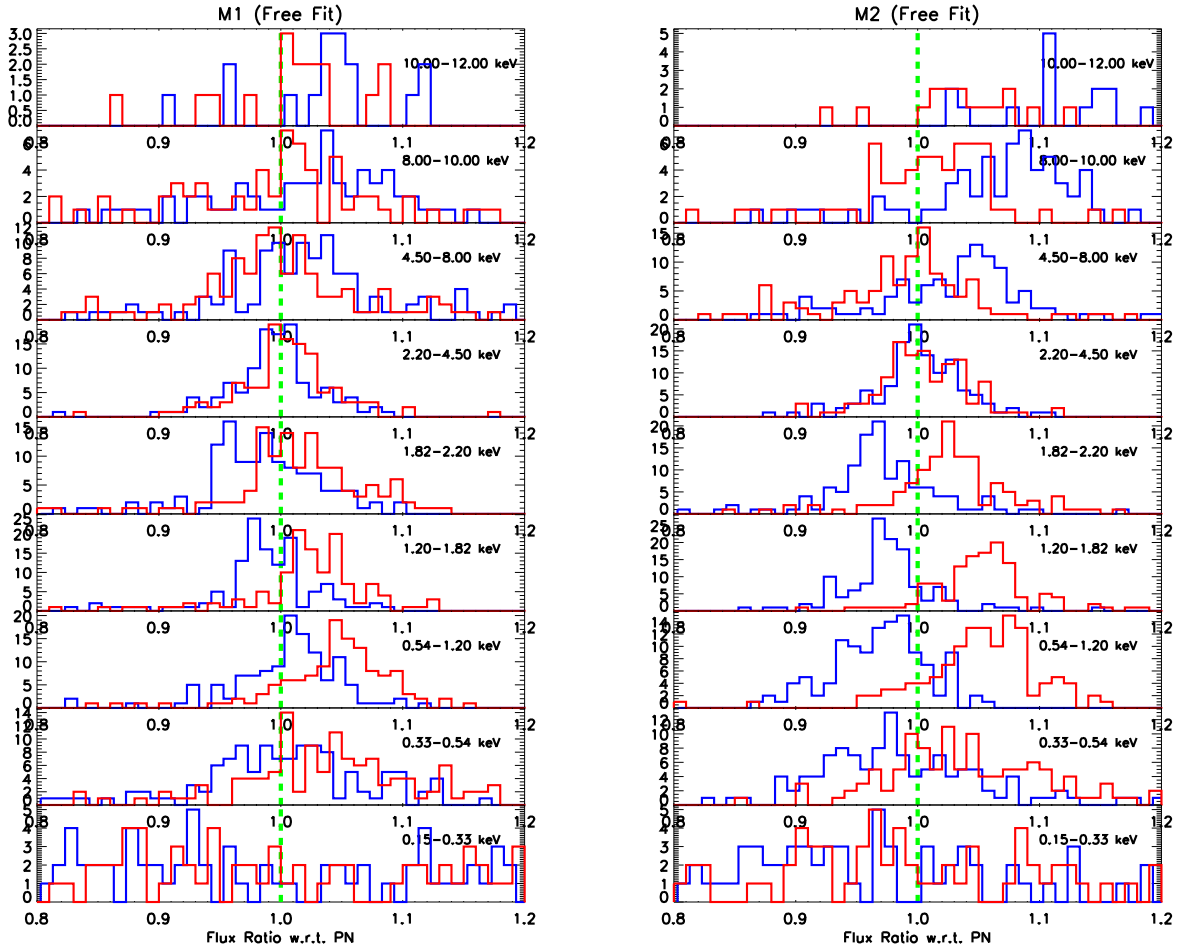


Figure 6: MOS-to-pn flux ratio histograms, analogous to Fig 3, with as difference that here the blue histogram shows results obtained with the original CORRAREA correction.

# 7 References

[1] Guainazzi, M. et al., 2014, XMM-CAL-SRN-0321
(https://xmmweb.esac.esa.int/docs/documents/CAL-SRN-0321-1-2.pdf)

[2] Read, A., et al., 2014, A&A, 564, 75

[3] Rosen, S., Webb, N., Watson, M., et al., 2016, A&A, 590, 1

Table 1: List of observations used in the derivation of the CORRAREA correction. Instrument modes are denoted by FF, LW and SW for Full Frame, Large Window and Small Window modes, respectively. Filters are denoted by Tn, Md and Tk for Thin, Medium and Thick filters, respectively.

| ObsID | Rev | Source Name | pn | | | MOS1 | | | MOS2 | | |
|---|---|---|---|---|---|---|---|---|---|---|---|
| | | | Exp | Mode | Filter | Exp | Mode | Filter | Exp | Mode | Filter |
| 0006220201 | 0197 | NGC 4507 | S003 | FF | Md | S001 | FF | Tk | S002 | FF | Tk |
| 0029340101 | 0238 | SV Cam | S003 | LW | Md | S001 | LW | Md | S007 | LW | Md |
| 0029340101 | 0238 | SV Cam | U003 | LW | Md | U003 | LW | Md | U003 | LW | Md |
| 0067750101 | 0311 | Cen X-4 | U002 | FF | Tn | S001 | FF | Tn | S002 | FF | Tn |
| 0084140501 | 0395 | MS0205.7+3509 | S001 | FF | Tn | S002 | FF | Md | S003 | FF | Md |
| 0086360401 | 0230 | V410 Tau | U002 | FF | Md | S005 | FF | Md | S006 | FF | Md |
| 0090070101 | 0462 | Q 0144-3938 | S003 | FF | Md | S001 | LW | Md | S002 | LW | Md |
| 0092850501 | 0373 | PG 1407+265 | S003 | FF | Tn | S001 | FF | Tn | S002 | FF | Tn |
| 0101040301 | 0178 | NGC 3227 | S003 | FF | Md | S001 | FF | Md | S002 | FF | Md |
| 0106860101 | 0157 | NGC 1313 | U002 | FF | Md | U003 | FF | Md | U003 | FF | Md |
| 0109080301 | 0443 | PG 1322+659 | S003 | LW | Tn | S001 | LW | Tn | S002 | LW | Tn |
| 0109080501 | 0549 | PG 1415+451 | S003 | LW | Tn | S001 | LW | Tn | S002 | LW | Tn |
| 0109080601 | 0489 | PG 1444+407 | S003 | LW | Tn | S001 | LW | Tn | S002 | LW | Tn |
| 0109080701 | 0444 | PG 1048+342 | S003 | LW | Tn | S001 | LW | Tn | S002 | LW | Tn |
| 0109080901 | 0453 | PG 1427+480 | S003 | LW | Tn | S001 | LW | Tn | S002 | LW | Tn |
| 0111251501 | 0422 | EUVE J2115.7-584 | S001 | LW | Tn | S002 | SW | Tn | S005 | SW | Tn |
| 0111290601 | 0482 | PG 1425+267 | S003 | FF | Tn | S001 | FF | Tn | S002 | FF | Tn |
| 0114090101 | 0051 | PKS 0537-286 | S006 | FF | Md | S002 | LW | Md | S004 | FF | Md |
| 0151390101 | 0630 | 4C +06.41 | S009 | FF | Tn | S007 | FF | Tn | S008 | FF | Tn |
| 0152940101 | 0660 | NGC 5252 | S003 | FF | Tn | S001 | FF | Tn | S002 | FF | Tn |
| 0200910101 | 0944 | 3C 109 | S003 | LW | Md | S001 | LW | Md | S002 | LW | Md |
| 0202860101 | 0902 | NGC 7172 | S003 | LW | Tn | S001 | LW | Tn | S002 | LW | Tn |
| 0203770201 | 0842 | PG 1416-129 | S003 | LW | Tn | S001 | LW | Tn | S002 | LW | Tn |
| 0205390301 | 0831 | PG 1351+64 | S003 | FF | Md | S001 | FF | Md | S002 | FF | Md |
| 0205770101 | 0738 | Z Cha | S003 | FF | Tn | S001 | LW | Tn | S002 | LW | Tn |
| 0300240501 | 1129 | ESO 323-G77 | S003 | FF | Tn | S001 | FF | Tn | S002 | FF | Tn |
| 0300480301 | 1081 | OJ 287 | U002 | LW | Md | U002 | LW | Md | U002 | LW | Md |
| 0302900101 | 1117 | NGC 5408 X-1 | S003 | FF | Tn | S001 | FF | Tn | S002 | FF | Tn |
| 0305920201 | 1096 | SDSS J114008.71+030711.4 | S003 | FF | Tn | S001 | FF | Tn | S002 | FF | Tn |
| 0306630101 | 1101 | LBQS 1228+1116 | S003 | FF | Tn | S001 | FF | Md | S002 | FF | Md |
| 0306630201 | 1103 | LBQS 1228+1116 | S003 | FF | Tn | S001 | FF | Md | S002 | FF | Md |
| 0400200101 | 1288 | PG 1402+261 | S003 | LW | Md | S001 | LW | Md | S002 | LW | Md |
| 0401060201 | 1271 | OJ 287 | S001 | LW | Md | S002 | LW | Md | S003 | LW | Md |
| 0405090101 | 1255 | NGC 1313 | S003 | FF | Md | S001 | FF | Md | S002 | FF | Md |
| 0405690201 | 1272 | NGC 5204 X-1 | S003 | FF | Md | S001 | FF | Md | S002 | FF | Md |
| 0405690501 | 1275 | NGC 5204 X-1 | S003 | FF | Md | S001 | FF | Md | S002 | FF | Md |
| 0500750101 | 1483 | NGC 5408 X-1 | S003 | FF | Tn | S001 | FF | Tn | S002 | FF | Tn |
| 0502220301 | 1441 | APM 08279+5255 | U002 | FF | Md | S001 | FF | Md | S002 | FF | Md |
| 0502630201 | 1533 | OJ 287 | S001 | LW | Md | S002 | LW | Md | S003 | LW | Md |
| 0506200301 | 1360 | 1H 0707-495 | S003 | LW | Md | S001 | SW | Md | S002 | SW | Md |
| 0550970101 | 1609 | PKS 1549-79 | S003 | FF | Md | S001 | LW | Md | S002 | LW | Md |
| 0553300301 | 1667 | NGC 1052 | S001 | FF | Md | S002 | FF | Md | S003 | FF | Md |
| 0553300401 | 1772 | NGC 1052 | S001 | FF | Md | S002 | FF | Md | S003 | FF | Md |
| 0554710801 | 2032 | 1H 0707-495 | S003 | LW | Md | S001 | SW | Md | S002 | SW | Md |
| 0555650201 | 1598 | VV Sco | U002 | FF | Md | S001 | FF | Md | S002 | FF | Md |
| 0560180701 | 1632 | EXO 0748-676 | S003 | FF | Md | S001 | FF | Md | S002 | FF | Md |
| 0561580401 | 1885 | Holmberg II X-1 | S001 | FF | Md | S002 | FF | Md | S003 | FF | Md |
| 0601400201 | 2198 | GRB 111209A | S003 | FF | Md | S001 | LW | Md | S002 | LW | Md |
| 0601560201 | 1737 | NGC 3660 | S003 | LW | Md | S001 | LW | Md | S002 | LW | Md |

Table 1: *continued*

| ObsID | Rev | Source Name | pn | | | MOS1 | | | MOS2 | | |
|---|---|---|---|---|---|---|---|---|---|---|---|
| | | | Exp | Mode | Filter | Exp | Mode | Filter | Exp | Mode | Filter |
| 0602290101 | 1723 | 11 LMi | S003 | FF | Tk | S001 | FF | Tk | S002 | FF | Tk |
| 0602490101 | 1744 | DK Cet | S003 | LW | Md | S001 | LW | Md | S002 | LW | Md |
| 0604060101 | 1842 | RBS 1955 | S003 | FF | Tn | S001 | FF | Tn | S002 | FF | Tn |
| 0605090101 | 1769 | XSS J05054-2348 | S003 | FF | Tn | S001 | FF | Tn | S002 | FF | Tn |
| 0605560401 | 1698 | EXO 0748-676 | U002 | FF | Tn | U002 | FF | Tn | U002 | FF | Tn |
| 0605560501 | 1751 | EXO 0748-676 | S003 | FF | Tn | S001 | FF | Tn | S002 | FF | Tn |
| 0606150101 | 1746 | PG 1126-041 | S003 | FF | Md | S001 | FF | Md | S002 | FF | Md |
| 0651690101 | 1927 | EXO 0748-676 | S003 | FF | Tn | S001 | FF | Tn | S002 | FF | Tn |
| 0651690101 | 1927 | EXO 0748-676 | U002 | FF | Tn | U003 | FF | Tn | U002 | FF | Tn |
| 0653380301 | 1943 | NGC 5408 X-1 | S003 | FF | Tn | S001 | FF | Tn | S002 | FF | Tn |
| 0653380401 | 2039 | NGC 5408 X-1 | S003 | FF | Tn | S001 | FF | Tn | S002 | FF | Tn |
| 0670880501 | 2263 | 3C 215 | S003 | FF | Md | S001 | FF | Md | S002 | FF | Md |
| 0672130101 | 2115 | M32 | S002 | FF | Tn | S001 | FF | Tn | S003 | FF | Tn |
| 0672130601 | 2119 | M32 | S002 | FF | Tn | U002 | FF | Tn | U002 | FF | Tn |
| 0672130701 | 2120 | M32 | S002 | FF | Tn | S001 | FF | Tn | S003 | FF | Tn |
| 0672530301 | 2104 | Zw 229.015 | S003 | LW | Md | S001 | SW | Md | S002 | SW | Md |
| 0673270101 | 2121 | J1633+4718 | S003 | LW | Tn | S001 | LW | Tn | S002 | LW | Tn |
| 0673270201 | 2154 | J1633+4718 | S003 | LW | Tn | S001 | LW | Tn | S002 | LW | Tn |
| 0673580201 | 2127 | IRAS 13224-3809 | S003 | LW | Tn | S001 | LW | Tn | S002 | LW | Tn |
| 0673580401 | 2131 | IRAS 13224-3809 | S003 | LW | Tn | S001 | LW | Tn | S002 | LW | Tn |
| 0673730101 | 2100 | PMN J0948+0022 | S003 | LW | Md | U002 | LW | Md | U002 | LW | Md |
| 0673730101 | 2100 | PMN J0948+0022 | S003 | LW | Md | U003 | LW | Md | U003 | LW | Md |
| 0690200301 | 2425 | HD 144217 | S003 | FF | Tk | S001 | FF | Tk | S002 | FF | Tk |
| 0690330101 | 2445 | EXO 0748-676 | S003 | FF | Tn | S001 | FF | Tn | S002 | FF | Tn |
| 0690600401 | 2298 | XBo 135 | U014 | FF | Tn | S001 | FF | Tn | S002 | FF | Tn |
| 0690870501 | 2504 | Mkn 1048 | S003 | SW | Tn | S001 | SW | Tn | S002 | SW | Tn |
| 0691100201 | 2384 | 2MASXJ06192755-6 | S003 | FF | Tn | S001 | FF | Tn | S002 | SW | Md |
| 0700381801 | 2353 | SXP1062 | S003 | FF | Tn | S001 | FF | Md | S002 | FF | Md |
| 0701780101 | 2458 | NGC 2992 | S003 | SW | Md | S001 | SW | Md | S005 | SW | Md |
| 0720110501 | 2487 | NGC 5548 | S003 | SW | Tn | S001 | SW | Tn | S002 | SW | Tn |
| 0720110701 | 2491 | NGC 5548 | S003 | SW | Tn | S001 | SW | Tn | S002 | SW | Tn |
| 0720110801 | 2493 | NGC 5548 | S003 | SW | Tn | S001 | SW | Tn | S002 | SW | Tn |
| 0720111001 | 2495 | NGC 5548 | S003 | SW | Tn | S001 | SW | Tn | S002 | SW | Tn |
| 0720111201 | 2497 | NGC 5548 | S003 | SW | Tn | S001 | SW | Tn | S002 | SW | Tn |
| 0720111401 | 2499 | NGC 5548 | S003 | SW | Tn | S001 | SW | Tn | S002 | SW | Tn |
| 0720111601 | 2593 | NGC 5548 | S003 | SW | Tn | S001 | SW | Tn | S002 | SW | Tn |
| 0720280101 | 2599 | IGR J14488-4008 | S003 | FF | Tn | S001 | FF | Tn | S002 | FF | Tn |
| 0721110101 | 2569 | Fairall 9 | U002 | SW | Md | U002 | SW | Md | U002 | SW | Md |
| 0721220101 | 2587 | IRAS 17020+4544 | S003 | SW | Md | S001 | SW | Md | S002 | SW | Md |
| 0721220301 | 2588 | IRAS 17020+4544 | S003 | SW | Md | S001 | SW | Md | S002 | SW | Md |
| 0722610101 | 2530 | IRAS F05189-2524 | S003 | FF | Md | S001 | FF | Md | S002 | FF | Md |
| 0724820101 | 2516 | IRAS 18325-5926 | S003 | SW | Tn | S001 | SW | Tn | S002 | SW | Tn |
| 0724820201 | 2537 | IRAS 18325-5926 | U002 | SW | Tn | U002 | SW | Tn | U002 | SW | Tn |
| 0727960301 | 2486 | QSO J1131-1231 | S003 | SW | Tn | S001 | SW | Tn | S002 | SW | Tn |
| 0740610201 | 2691 | V1261 Ori | S003 | FF | Tk | S001 | FF | Tk | S002 | FF | Tk |
| 0741260101 | 2667 | HE 1136-2304 | S003 | SW | Tn | S001 | SW | Tn | S002 | SW | Tn |
| 0741390101 | 2650 | RX J0439.6-5311 | S003 | SW | Md | S001 | SW | Md | S002 | SW | Md |
| 0741390201 | 2662 | RX J1355.2+5612 | S003 | SW | Md | S001 | SW | Md | S002 | SW | Md |
| 0741390401 | 2667 | RX J1355.2+5612 | S003 | SW | Md | S001 | SW | Md | S002 | SW | Md |
| 0742490101 | 2803 | SN 1978K | S003 | FF | Md | S001 | FF | Md | S002 | FF | Md |
| 0743830501 | 2765 | NGC 985 | S003 | SW | Tn | S001 | SW | Tn | S002 | SW | Tn |
| 0744240101 | 2682 | QSO B1422+231 | S003 | FF | Tn | S001 | FF | Tn | S002 | FF | Tn |
| 0744290101 | 2789 | Mrk 493 | S003 | SW | Md | S001 | SW | Md | S002 | SW | Md |
| 0744440101 | 2753 | PG 1244+026 | S003 | SW | Tn | S001 | SW | Tn | S002 | SW | Tn |

Table 1: *continued*

| ObsID | Rev | Source Name | pn | | | MOS1 | | | MOS2 | | |
|---|---|---|---|---|---|---|---|---|---|---|---|
| | | | Exp | Mode | Filter | Exp | Mode | Filter | Exp | Mode | Filter |
| 0744440201 | 2754 | PG 1244+026 | S003 | SW | Tn | S001 | SW | Tn | S002 | SW | Tn |
| 0744440501 | 2766 | PG 1244+026 | S003 | SW | Tn | S001 | SW | Tn | S002 | SW | Tn |
| 0744450101 | 2673 | RBS 1055 | S003 | LW | Tn | S001 | LW | Tn | S002 | LW | Tn |
| 0744450301 | 2773 | RBS 229 | S003 | LW | Tn | S001 | LW | Tn | S002 | LW | Tn |
| 0744490401 | 2744 | Mrk 915 | S003 | LW | Tn | S016 | LW | Tn | S002 | LW | Tn |
| 0744490501 | 2746 | Mrk 915 | S003 | LW | Tn | S001 | LW | Tn | S002 | LW | Tn |
| 0744500201 | 2689 | T Tau | S003 | FF | Md | S001 | FF | Md | S002 | LW | Md |
| 0761220101 | 2853 | NGC 5506 | U002 | SW | Tn | U002 | SW | Tn | U002 | SW | Tn |
| 0761500201 | 2822 | OJ 287 | S003 | LW | Tn | S001 | LW | Tn | S002 | LW | Tn |
| 0764010101 | 2929 | MCG-03-58-007 | S003 | FF | Tn | U002 | FF | Tn | U002 | FF | Tn |
| 0764010101 | 2929 | MCG-03-58-007 | S003 | FF | Tn | U003 | FF | Tn | U003 | FF | Tn |
| 0764170101 | 2851 | TON S 180 | S004 | SW | Tn | S002 | SW | Md | S003 | SW | Tn |
| 0764370201 | 2914 | QSO B2202-209 | S003 | FF | Tn | S001 | FF | Md | S002 | FF | Md |
| 0780561301 | 3038 | IRAS 13224-3809 | S002 | LW | Tn | S001 | LW | Tn | S005 | LW | Tn |
| 0780561701 | 3045 | IRAS 13224-3809 | S002 | LW | Tn | S001 | LW | Tn | S005 | LW | Tn |
| 0792180101 | 3046 | IRAS 13224-3809 | S002 | LW | Tn | U002 | LW | Tn | U002 | LW | Tn |
| 0792180301 | 3049 | IRAS 13224-3809 | S002 | LW | Tn | U002 | LW | Tn | U002 | LW | Tn |